Molecular Dynamics Simulations of Phospholipid Bilayers: Influence of Artificial Periodicity, System Size, and Simulation Time

Alex H. de Vries,*,† Indira Chandrasekhar, Wilfred F. van Gunsteren, and Philippe H. Hünenberger

Laboratory of Physical Chemistry, ETH, ETH Hönggerberg, CH-8093 Zürich, Switzerland

Received: February 15, 2005; In Final Form: April 5, 2005

This article investigates the convergence of structural and dynamical properties with system size and with time in molecular dynamics simulations of solvated phospholipid bilayers performed at constant volume under periodic boundary conditions using lattice-sum electrostatics. The electron density profile across the bilayer, the carbon−deuterium order parameters, and the surface tension are shown to be converged for a bilayer containing 36 lipids per leaflet and simulated over a period of 3−4 ns. Reasonable estimates for these properties can already be obtained from a system containing 16 lipids per leaflet. The convergence limit of 36 lipids per leaflet and the investigation of the correlation between lipid headgroup dipoles suggest a correlation length of about 3−5 nm in the lateral directions for a hydrated DPPC bilayer in the liquid-crystalline phase. Although these (relatively small) system sizes and (relatively short) time scales appear sufficient to obtain converged collective structural properties at constant volume, two restrictions should be kept in mind: (i) the relaxation times associated with the motion of individual lipids may be much longer and (ii) simulated properties converge significantly faster under constant volume conditions as compared to constant pressure conditions. Therefore, an accurate assessment of the dynamical properties of the system or of the relaxation of the bilayer under constant pressure conditions may require longer simulation time scales.

Introduction

Molecular dynamics (MD) simulations of lipid bilayer systems have become an established tool in developing a fundamental understanding of their properties.[1] Model calculations are used to interpret and guide experiments, providing the complementary microscopic view to macroscopic observations.[2−6] However, when performing atomistic simulations with an explicit representation of the solvent molecules, the finite computational resources impose a serious limitation on both the length scales and the time scales accessible by this approach. One of the recurring questions when interpreting the results of these simulations is whether the simulated system is large enough and has been sampled for a long enough period of time to enable fair comparison with experiment. As part of the ongoing development of the field, a number of studies concerned with this problem of the required length scales[7−10] and time scales[11,12] have appeared recently.

Most previous studies of the dependence of simulated lipid bilayer properties on system size and simulation length have focused on the area per lipid of a dipalmitoylphosphatidylcholine (DPPC) bilayer in water. The experimental properties that are most readily available for lipid bilayers (electron density profiles from X-ray diffraction, and carbon−deuterium order parameters (S_{CD}) from ^{2}H NMR quadrupole splittings) generally correlate well with this single property. Lindahl and Edholm[8] showed that the area per lipid for a fully hydrated DPPC bilayer increases from 0.620 nm^2 for a system containing 32 lipids per leaflet of the bilayer to 0.635 nm^2 for a system with 512 lipids per leaflet, using a straight cutoff technique for the evaluation of electrostatic interactions. The dependence was found to be weaker when using Ewald summation to evaluate electrostatic interactions.[10] Feller and Pastor[7] reported a decrease in the surface tension upon increasing the system size in constant surface area simulations of DPPC bilayers under stress. Size effects were also studied by Marrink and Mark,[9] who simulated a hydrated bilayer of glycerol monoolein, using both constant surface tension and constant surface area conditions. They observed that for stress-free bilayers the area per lipid does not significantly vary with the system size in the range of lateral dimensions considered (5−20 nm). However, they noted that the correlation times in the calculated surface areas or surface tensions were of the order of 0.5 ns, and suggested that the length of any simulation should be at least a few multiples of this correlation time. Correlation times of up to 2.5 ns in the calculated surface area were found by Anézo et al.[11] for hydrated DPPC bilayers, considering systems containing 64−128 lipids per leaflet under constant pressure conditions, and simulated for up to 100 ns. Comparatively longer relaxation times (up to 20 ns) were found necessary to reach the equilibrium area per lipid, depending on the starting conditions. The simulations of a solvated DPPC bilayer by Patra et al.[12] gave a similar picture. Despite these recent investigations, a systematic study of finite-size effects over a large range of system sizes, including very small systems, has not yet been undertaken. Although in the early literature small patches of bilayers were simulated, the minimum size was still 24−32 lipids per leaflet[13−15] and finite-size effects could not be assessed.

In the present study, DPPC bilayer systems with periodic unit cells containing 1−64 lipids per leaflet are investigated, bridging into the literature for larger systems. To ensure a strict comparability between the systems, electrostatic interactions are evaluated by using a lattice-sum method, applied in such a way

* Address correspondence to this author.

† Present address: Molecular Dynamics Group, Biophysical Chemistry, University of Groningen, Nijenborgh 4, 9747 AG Groningen, The Netherlands. E-mail: a.h.de.vries@rug.nl.

10.1021/jp0507952 CCC: $30.25
Published on Web 05/14/2005

that the long-range interactions are treated identically and with a similar accuracy for all systems. In this way, any difference in the simulated properties results solely from finite-size effects and artificial periodicity. The main purpose of this investigation is to find the minimum system size required to obtain converged structural and dynamical properties within the chosen force field and simulation conditions. A second purpose is to gain insight into the nature of these finite-size effects, which should help in choosing appropriate simulation conditions for future studies.

The adequacy of using lattice-sum methods to compute electrostatic interactions in (bio-)molecular simulations is a subject of ongoing discussions (for a recent summary, see ref 16). Lattice-sum methods treat long-range electrostatic interactions as exactly periodic within a system consisting of the unit cell and an infinite array of translated replicas. Although this approach is certainly reasonable in the context of crystal simulations, it is clearly an approximation when considering dilute solutions, and may lead to so-called finite-size effects. These effects are likely to be important[17−20] for systems involving (i) a solvent of low dielectric permittivity, (ii) a large low-dielectric solute cavity (compared to the unit cell size), and (iii) a nonneutral or highly polar solute. Clearly, hydrated lipid bilayers present the second and third characteristics because they consist of a large low-dielectric volume (acyl chains in the bilayer interior) surrounded by a highly polar interface (Zwitterionic headgroups). In the specific context of bilayers, finite-size effects due to the use of lattice-sum electrostatics are expected to be of three kinds: (i) artificial interactions between periodic copies of the bilayer in the longitudinal (bilayer stacking) direction; (ii) perturbation of the solvating water molecules through interaction with the copies of the bilayer in the longitudinal direction; and (iii) enforcement of artificial long-range (periodicity-induced) lipid−lipid spatial correlations in the lateral (bilayer plane) directions. The spatial correlations in the lateral directions are dictated by the dimensions of the unit cell in the bilayer plane, which impose periodicity constraints on the system. The present study only assesses the sensitivity of the bilayer properties to the third type of effects, because the unit cells considered differ only in their lateral dimensions. A similar approach was applied previously to study finite-size effects down to a single molecule in the periodic unit cell for pure water.[21] In this case infinite-size limits were essentially reached for the heat of vaporization, the density (at constant pressure), and the pressure (at constant volume) for cubic boxes of edge length 3 nm (∼1000 molecules). For the self-diffusion coefficient, the infinite-size limit appeared not to have been reached for boxes of edge length 5 nm.

Computational Details

All simulated systems consisted of molecules of the lipid DPPC with water as a solvent. The DPPC molecule is a triester of glycerol. The hydroxyl groups on the first and second carbon atoms are esterified with palmitic acid chains (16 carbon saturated unbranched carboxylic acid; the carbons are numbered from 1 to 16 starting from the carboxylate carbon), referred to as the sn-1 and sn-2 chains, respectively. The hydroxyl group on the third carbon is esterified with a Zwitterionic phosphocholine group (formal negative and positive charges on the phosphate on the trimethylamino groups, respectively), referred to as the lipid headgroup. The force-field parameters used for DPPC molecules (GROMOS 45A3_C95 force field[22]) and for water (SPC model[23]) have been described previously in the literature. The simulations were performed with a modified version of the GROMOS96 program.[24,25] The smallest unit cell contained 2 DPPC and 60 water molecules. This unit cell was constructed from a snapshot of an equilibrated bilayer system containing 128 lipids and 4480 water molecules, by selecting two lipids in opposite leaflets of the bilayer that were approximately located at the same lateral position, together with a column of 60 water molecules from the same region. This system was then subjected to energy minimization and equilibration. Larger unit cells were built from the resulting equilibrated configuration, by replicating the system a number of times in both lateral directions. The unit cells generated by this procedure, which contained 1, 4, 9, 16, 36, or 64 copies of the smallest unit cell, were squares in the lateral directions and shared a common length in the longitudinal direction. These numbers also correspond to the number of lipid molecules in one leaflet of the bilayer, and will be used to label and discuss the resulting simulations. All simulations were performed under periodic boundary conditions and at constant volume (fixed unit-cell dimensions). The length of the box in the longitudinal (bilayer stacking) direction was 6.7 nm in all simulations, which corresponds to the spacing at full hydration evaluated from X-ray scattering data.[26] The length of the box in the lateral directions was a multiple of 0.8 nm, which is the value for the smallest unit cell containing a single pair of DPPC molecules. Thus, all systems were simulated at a projected area per lipid of 0.64 nm^2, which corresponds to the best currently available experimental value, estimated by combining volumetric and X-ray scattering data.[26]

The P^3M method[27] was used to compute electrostatic interactions. The reciprocal-space component was evaluated by using a grid spacing of 0.1 nm in all directions, an assignment function of order three,[28−31] a finite-difference operator of order three,[28−31] and a third-order truncated polynomial charge-shaping function of width 0.7 nm.[31] The real-space cutoff distance was set to the same value of 0.7 nm, and applied on the basis of interatomic distances. Tinfoil (conducting) boundary conditions were used, i.e., no extrinsic electrostatic potential contribution was included.[30,32] This setup resulted in an estimated (upper bound) root-mean-square error in the electrostatic forces of 1.2 $kJ\cdot mol^{-1}\cdot nm^{-1}$,[31] to be compared with typical magnitudes of the forces on atoms of about 10^3 $kJ\cdot mol^{-1}\cdot nm^{-1}$ for this system. van der Waals interactions were computed by using a twin-range cutoff scheme based on interatomic distances for the DPPC molecules and intermolecular (oxygen−oxygen) distances for the solvent. Interactions within a short-range cutoff distance of 0.9 nm were evaluated every step, whereas the interactions between the short-range cutoff distance and the long-range cutoff distance of 1.4 nm were evaluated every 5 steps and kept constant in between. The nonbonded pair list (which was also used for the evaluation of the real-space electrostatic interactions) was updated every 5 steps. The equations of motion were propagated with use of a Verlet leapfrog algorithm with a time step of 2 fs. Bond lengths were constrained by using the SHAKE algorithm[33] with a relative geometric tolerance of 10^{-4}. A Berendsen thermostat[34] was employed to couple the DPPC and solvent molecules to two separate temperature baths, both at a reference temperature of 323 K, and with a coupling constant of 0.1 ps.

The use of a common scheme (P^3M parameters and cutoff distances) to evaluate nonbonded interactions in all simulations ensures that the differences in the simulated properties are solely due to differences in the system size. However, the simulation of periodic unit cells with sizes that may be smaller than twice the maximal cutoff distance (1.4 nm) raises some implementation issues because the standard GROMOS96 code does not

allow for the interaction of an atom with multiple periodic copies of another one or of itself. Therefore, a special version of the GROMOS96 program was developed to deal with the smallest unit cells. The basic idea is to replicate the unit cell corresponding to the actual system (referred to as the real unit cell) as many times as needed to obtain a larger unit cell (referred to as the formal unit cell) of size larger than twice the maximal cutoff distance. The interactions within the formal unit cell may be handled through the normal GROMOS96 code. However, some care must be taken to preserve the periodicity of the real unit cells within the formal one. This is done by selecting initial coordinates and allocating random initial velocities that satisfy this periodicity requirement, and correcting for possible numerical deviations in the forces, velocities, and coordinates at each time step of the simulation. The simulations with 1 or 4 lipids per leaflet in the real unit cell were performed by using a formal unit cell containing 16 lipids per leaflet, and the simulation with 9 lipids per leaflet in the real unit cell was performed with a formal unit cell containing 36 lipids per leaflet. The lateral dimensions of these formal unit cells are 3.2 and 4.8 nm, respectively, which is larger than twice the maximal nonbonded cutoff distance of 1.4 nm. No special treatment was required for real unit cells containing at least 16 lipids per leaflet.

The systems were equilibrated for 0.5 ns and data were collected over at least 3 ns. Configurations from the trajectories were saved every 10 ps for analysis. The properties monitored were the electron density profile across the bilayer, the carbon−deuterium order parameters (S_{CD}) in the lipid tails, and the surface tension of the bilayer, as well as a number of time-correlation functions. The electron density profile across the bilayer was evaluated by averaging the atomic densities weighted by the associated number of electrons, collected in slices of 0.1 nm width in the longitudinal direction. S_{CD} is defined as $S_{CD}(i) = (3\langle\cos^2\theta_i\rangle - 1)/2$, where θ_i is the angle between a C−D vector of the ith methylene group in the lipid chain and the longitudinal axis of the system and the angular brackets denote ensemble averaging. Note that the force field used in the present work does not contain explicit aliphatic hydrogen (or deuterium) atoms,[22] but instead employs a united atom representation for methylene and methyl groups. Therefore the positions of the aliphatic deuterium atoms on the ith methylene group were reconstructed from the positions of the carbon atoms $i - 1$, i, and $i + 1$ along the chain, assuming a tetrahedral geometry at the ith carbon atom. The procedure also assumes equivalence of both C−D vectors through rotational averaging over the methylene segment.[13] The geometry of lipid bilayers is such that the angle between the C−D vectors in the acyl chain and the bilayer normal is 90° if the lipids are perfectly ordered in the bilayer. This situation corresponds to $S_{CD} = -1/2$. A value of $S_{CD} = 0$ corresponds to an orientation of the C−D vector that is either permanently at the magic angle or random. S_{CD} values for acyl chains in lipid bilayers are assumed to fall in the range −0.5 to 0 and are therefore usually reported as $-S_{CD}$ or $|S_{CD}|$. The surface tension γ was calculated from the pressure tensor components in the lateral ($P_{lat} = (P_{xx} + P_{yy})/2$) and longitudinal ($P_{zz}$) directions as $\gamma = L_z(P_{zz} - P_{lat})$, where L_z is the length of the box in the longitudinal direction. Because the pressure is a highly fluctuating property, it is useful to provide error bars in the calculated surface tensions. These were determined by block-averaging, using the information of the pressure tensor components calculated at every simulation step and saved as 10 ps block averages. The exact procedure employed to derive error bars at a 95% confidence interval from these data is detailed in the Appendix. Briefly stated, the procedure considers block averages as measurements with an associated error $\sigma_{95}{}^b$. As the block size is increased, $\sigma_{95}{}^b$ decreases. However, the error upon averaging over the different block averages, $\sigma_{95}{}^a$, concomitantly increases. The dependence of the combined error $\sigma_{95} = \sigma_{95}{}^a + \sigma_{95}{}^b$ on the block size may then be used to estimate an error accounting for the correlation in the data. Finally, the analysis of the simulations also involved the evaluation of the time-correlation functions ($C(t) = \langle A(\tau) \cdot A(\tau + t)\rangle_\tau$, where A is some time-dependent property) associated with the orientation of the vectors connecting specific atoms in the DPPC molecule, so as to investigate the relaxation behavior of the lipids in the system.

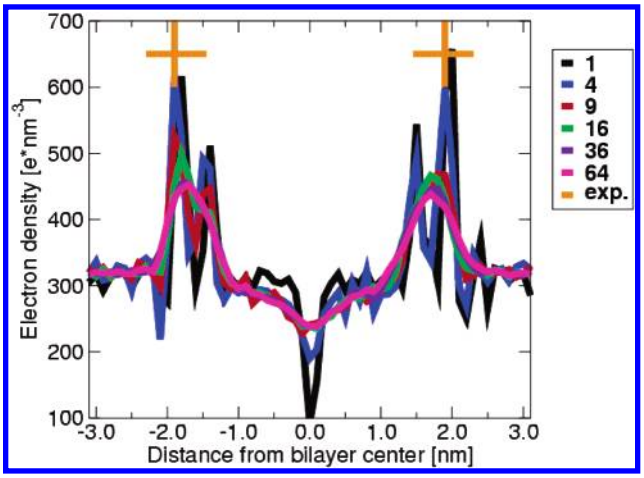

Figure 1. Electron density profiles across a hydrated DPPC bilayer, calculated for simulated systems of different sizes, and compared to experiment. The simulated systems involve 1 (black), 4 (blue), 9 (red), 16 (green), 36 (indigo), and 64 (magenta) lipids per leaflet. The bars drawn in orange indicate the position (vertical) and full width at half-maximum (horizontal) of the high-density peaks determined from X-ray scattering.[26] These bars are drawn at an arbitrary height.

Results and Discussion

A series of simulations was performed for hydrated DPPC bilayer systems under periodic boundary conditions containing 1, 4, 9, 16, 36, or 64 lipid molecules per leaflet together with 30 molecules of water per lipid in the unit cell. The simulations were performed with constant box lengths (longitudinal bilayer stacking distance 6.7 nm, area per lipid 0.64 nm^2). The electrostatic interactions were evaluated through a lattice-sum (P^3M) method. The parameters determining the evaluation of nonbonded interactions were rigorously identical for all systems, so that differences in the monitored properties arise exclusively from finite-size effects and artificial periodicity.

Figure 1 shows the electron density profiles across the bilayer, calculated for the series of systems considered. The positions and full width at half-maximum of the high-density peaks in the experimental density profiles determined by X-ray diffraction[26] are also shown for comparison. For all simulated systems, the electron dense regions of the bilayer are well positioned compared to experiment. The electron density in the water−lipid interface regions located at about 1.5−2.0 nm from the bilayer mid-plane is, however, considerably more structured for the smallest systems, showing two peaks rather than a single broad one. A single broad peak (consistent with experiment) is found for systems involving at least 36 lipids per leaflet. The smallest systems are also characterized by a deep methyl trough at the center of the bilayer, typically indicative of a bilayer system in the gel phase.[6,35]

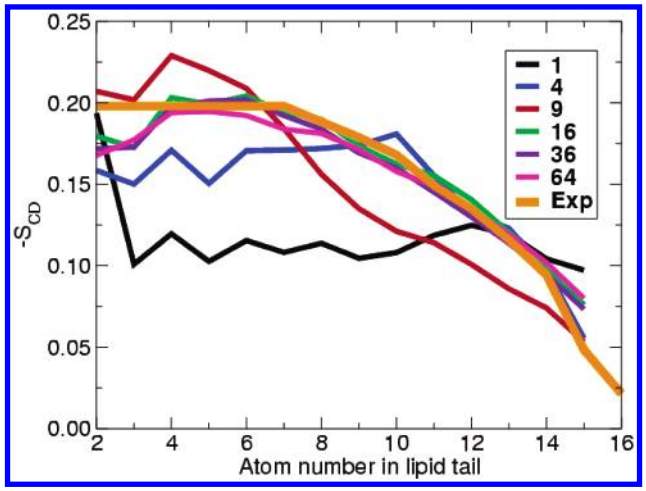

Figure 2. S_{CD} profiles for the acyl chains of a hydrated DPPC bilayer, calculated for simulated systems of different sizes, and compared to experiment. The S_{CD} values are averaged over both chains in a lipid and over all lipids in the system. The numbering follows the sequence from the ester carbon to the terminal methyl group of the chain. The color scheme is the same as in Figure 1. The orange profile was determined experimentally by Petrache et al.[36]

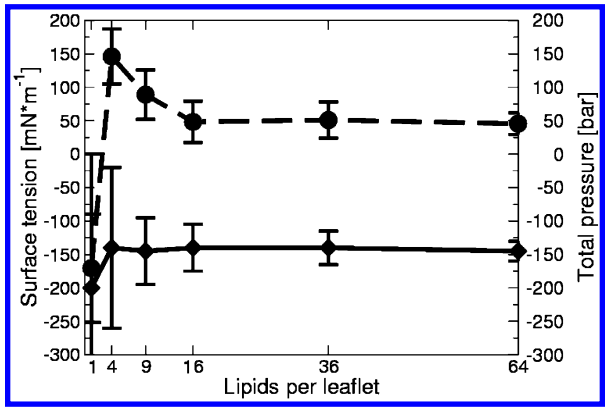

Figure 3. Surface tension (left scale and dashed line) and total pressure (right scale and solid line) of a hydrated DPPC bilayer, calculated for simulated systems with different numbers of lipids per leaflet. The error bars are drawn at the 95% confidence interval determined by a block averaging procedure (see the Appendix).

The S_{CD} profiles of the lipid acyl chains (averaged over both chains in a lipid and over all lipids in the system) are presented in Figure 2, together with the experimental profile determined by Petrache et al.[36] The S_{CD} profiles are found to strongly depend on the system size up to a size of 16 lipids per leaflet. For larger system sizes, the S_{CD} profiles are consistent among each other and with experiment. Note that the calculated S_{CD} values are somewhat lower than the experimental ones for the first few methylene groups, which are closest to the bilayer surface. This feature has also been observed in experiment involving specific deuteration of the C2 methylene group of the sn-2 chain.[37] However, the signals of the first six methylene groups were not resolved in the experiments of Petrache et al.,[36] who used perdeuterated chains.

Figure 3 shows the surface tension in the bilayer and the total pressure in the system as a function of the number of lipids per leaflet in the unit cell. The two quantities determine the directions in which the box dimensions would evolve in a simulation under constant pressure or constant surface tension conditions. The surface tension measures the intrinsic tendency of the bilayer lateral dimensions to change relative to the longitudinal one, while the total pressure measures the tendency of the three dimensions to change simultaneously. A positive surface tension indicates that the system tends to a lateral shrinkage and a longitudinal expansion. A zero surface tension indicates that the system is at equilibrium with respect to its surface area and stacking distance for a particular pressure. The surface tension is positive (except for the smallest system), which shows that most systems tend to a lateral shrinkage. This is consistent with the fact that the equilibrium area per lipid within the force field employed is significantly smaller (0.57 nm^2)[22,38] than the fixed area (0.64 nm^2) used in the present simulations. The surface tension converges to a value of about 50 $mN \cdot m^{-1}$ for systems containing at least 16 lipids per leaflet. The total pressure is negative for all simulated systems, and converges to a value of about −140 bar for systems containing at least 4 lipids per leaflet. The behavior of the smallest system is qualitatively different in that it tends to a relative lateral expansion. A more detailed analysis of the pressure tensor shows that this behavior is largely due to a considerably more negative longitudinal pressure component compared to the larger systems, together with somewhat less negative lateral components.

The results presented above provide a clear-cut answer to the question of the minimum system size required for obtaining converged structural properties of a fully hydrated DPPC bilayer simulated at constant volume. The minimum system size for the reliable calculation of the structural properties monitored (i.e. those most readily available from experiment) is 36 lipids per leaflet, while reasonable estimates for these properties are already obtained from a system as small as 16 lipids per leaflet (Figures 1−3). This information may prove extremely useful for purposes of force field development and refinement. It suggests that inexpensive explorations of force-field parameters and simulation conditions may be performed for relatively small systems simulated at constant volume. For example, such simulations could be performed to adjust force-field parameters so as to bring the total pressure close to 1 bar and the surface tension close to 0 at the experimental value for the projected area per lipid. Of course, this approach should be followed by further refinement with larger systems, and by simulations under constant pressure or constant surface tension conditions, to ensure the development of a generally applicable force field.

In principle, the magnitudes of the surface tension and total pressure computed under constant volume conditions could be used to obtain an estimate for the equilibrium area and stacking distance under constant pressure conditions, or for the applied surface tension required to ensure a certain area per lipid. For the present force field and with reaction-field electrostatics,[39] it is known that under constant pressure conditions of 1 bar and no applied surface tension, the area per lipid is considerably smaller (0.57 nm^2)[22] than the constant area imposed in the present simulations (0.64 nm^2). However, the application of a surface tension of -30 $mN \cdot m^{-1}$ together with a longitudinal pressure of 1 bar to a system containing 64 lipids per leaflet yielded an area per lipid of approximately 0.64 nm^2. Conversely, at a constant surface area of 0.64 nm^2 and a longitudinal pressure of 1 bar, the surface tension was found to be about 25 $mN \cdot m^{-1}$.[38] These results (from simulations with reaction-field electrostatics) are qualitatively consistent with the surface tension of about 50 $mN \cdot m^{-1}$ obtained in the present study for the largest systems.

The nature of finite-size effects in simulations of DPPC bilayers under periodic boundary conditions can be better characterized by considering the microscopic structure of the systems. Snapshots from the different simulations are shown in Figure 4. Expectedly, imposing artificial periodicity induces structure in the bilayer. The snapshots from the smallest systems

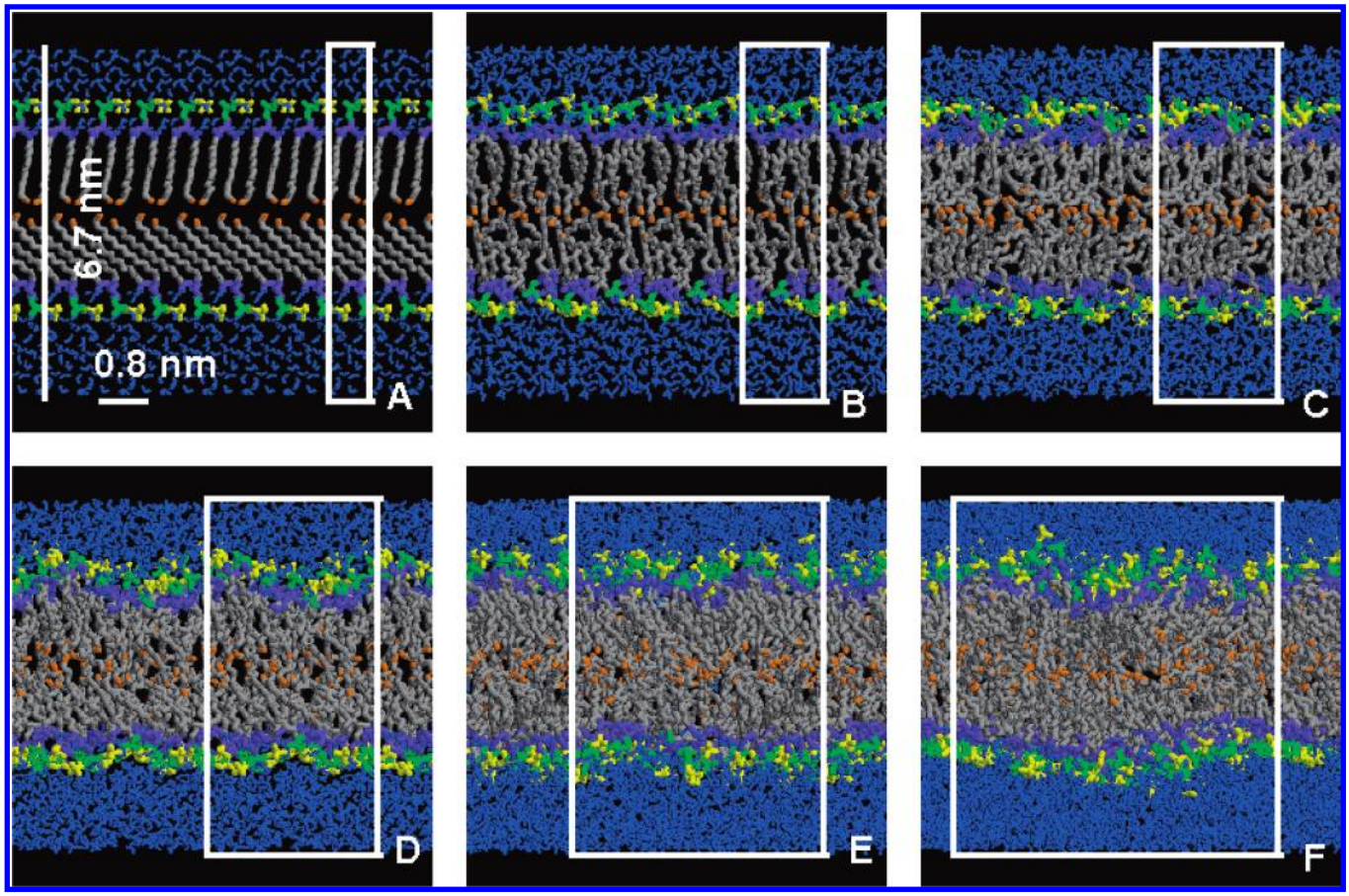

Figure 4. Snapshots taken at the end of MD simulations of a hydrated DPPC bilayer with different unit-cell sizes. The simulated systems involve 1 (A), 4 (B), 9 (C), 16 (D), 36 (E), and 64 (F) lipids per leaflet. Bonds are drawn as thick lines. Water is in blue, the choline moiety of the lipid headgroup in yellow, the phosphate moiety in green, the glycerol ester moiety in purple, the methylene groups of the lipid tails in gray, and the terminal methyl group in orange. The boundaries of the unit cell are indicated by white lines. The length scales are indicated by the bars in panel A.

are more characteristic of a DPPC bilayer in a gellike as opposed to a liquid-crystalline phase. This is reflected in the electron density and the S_{CD} profiles (Figures 1 and 2). The negative surface tension for the system with 1 lipid per leaflet is probably a consequence of the drastic geometrical constraints imposed by periodicity on the lipid−lipid interactions. However, the reason for the more positive surface tension (increased tendency for lateral shrinkage) upon decreasing the system size from 64 to 4 lipids per leaflet (Figure 3) is not entirely clear. One possible interpretation is that the artificial ordering induced by periodicity permits a more favorable packing of the chains or, equivalently, results in a more limited entropy loss upon increasing the packing density. Upon increasing the unit-cell size, the number of gauche defects in the acyl chains increases, and backfolding of the chains toward the bilayer−water interface occurs while the interior of the bilayer becomes more liquidlike. Finally, undulations of the bilayer[8] start to develop at a system size of 64 lipids per leaflet (Figure 4F). The transition between the gellike and liquid-crystalline phases occurs approximately for a system size of 36 lipids per leaflet, suggesting a lateral correlation length of about 5 nm in the liquid-crystalline phase (the box size in the lateral directions is 4.8 nm for the system containing 36 lipids per leaflet).

The strongest structural correlations in a DPPC bilayer are expected to be those associated with the interaction between the lipid headgroup dipoles. This correlation can be investigated by monitoring the cosine of the angle between the headgroup dipole vectors of two lipids as a function of the lipid−lipid distance. The result of this analysis, done separately for the two leaflets of the bilayer to provide an indication for convergence, is shown in Figure 5 for the different system sizes. In general, the profiles show anticorrelation of the dipoles at short distance (first neighbors), correlation at a slightly larger distance (second neighbors), and some further structure up to a distance of at

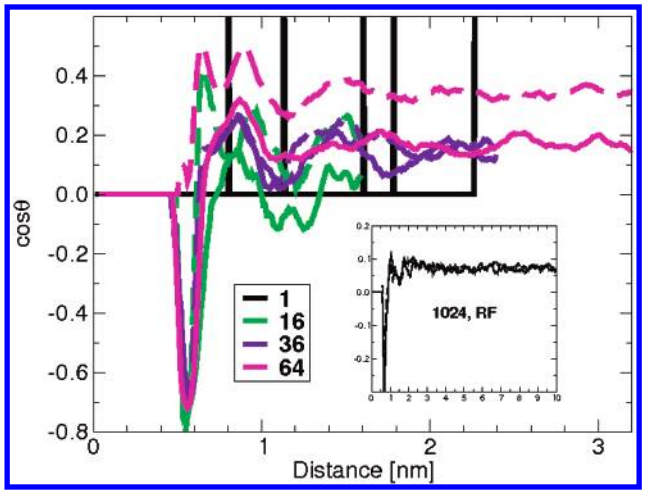

Figure 5. Cosine of the angle θ between the headgroup dipoles of two lipids as a function of lipid−lipid headgroup distance, calculated for DPPC bilayer systems of different sizes. The color scheme is the same as in Figure 1. For each system, curves are reported for the two leaflets of the bilayer separately (solid and dashed lines). The inset shows the corresponding curves for a system of 1024 lipids per leaflet (using reaction-field electrostatics).

least 3 nm. The interpretation of the profiles is complicated because favorable interactions between dipoles are achieved either by antiparallel alignment with perpendicular displacement (showing up as an anticorrelation) or by parallel alignment with parallel displacement (showing up as a correlation). The short-distance anticorrelation peak seen for most systems is indicative of the first type of arrangement. However, one of the two leaflets in the system containing 64 lipids per leaflet shows short-distance correlation instead, reflecting the dominance of the second type of arrangement in this leaflet. In view of the long relaxation times associated with headgroup reorientation (see below), it is not surprising that the two leaflets behave differently on the simulation time scale. Much longer simulations will be required for the leaflets to sample the same configurational space. Note finally that the correlation profiles do not necessarily converge to zero at large distances because the dipoles are on average tilted with respect to the bilayer normal, so that a longitudinal correlation may remain even when the lateral correlation vanishes. The distributions of the angles defined by headgroup dipoles relative to the bilayer normal are similar for all systems containing 9 lipids per leaflet or more (data not shown). The distributions are broad, with a maximum at around 90° and a skew to smaller angles (outward-directed dipoles). The smallest systems show narrower distributions compared to the larger systems. It appears from Figure 5 that the longest lateral correlation length between the headgroup dipoles in a DPPC−water system is at least 3 nm. The inset of Figure 5 shows the headgroup dipole−dipole correlation for a system containing 1024 lipids per leaflet, simulated by using reaction-field electrostatics. The correlation reaches its plateau value at around 4 nm and presents a very similar structure at shorter distances as that observed in the present lattice-sum simulations. Thus, the use of a much larger system size and of a simulation scheme that largely breaks the long-range electrostatic periodicity still leads to similar conclusions concerning the lateral correlation length in lipid bilayers.

The orientational behavior of the headgroups for different system sizes is illustrated in Figure 6. Here, the headgroup phosphorus and nitrogen atoms are shown as large balls and the atoms connecting these as thick bonds. The atoms in the two leaflets are colored differently. In the system containing 1 lipid per leaflet (Figure 6A), all lipids are translated replicas of each other. In this case, the most favorable orientation of the headgroup is reached when the dipole moment is aligned along the diagonal of the unit cell within the lateral plane. In addition, the headgroups in the two leaflets are shifted with respect to each other so as to minimize repulsive electrostatic interactions between the two leaflets. In the system containing 4 lipids per leaflet (Figure 6B) the headgroups of the lipids show a tendency to clustering, nearest neighbors being oriented either head against tail or parallel and shifted. Note also that the dipole moments of the two leaflets no longer point in the same direction. As the size of the unit cell is further increased (Figure 6C,D), the clustering of headgroups becomes more prominent. Viewed from the top, the headgroup distribution is seen to be rather inhomogeneous. This observation is not an artifact related to the system being simulated at a nonequilibrium area per lipid for the specific force field, and similar inhomogeneities are also seen at a smaller area per lipid (data not shown). The headgroup clusters are seen to reach a finite size in the largest system, i.e., favorable head-to-tail and shifted antiparallel arrangements no longer extend over the entire box. The snapshots in Figure 6 are in good qualitative agreement with the correlation length

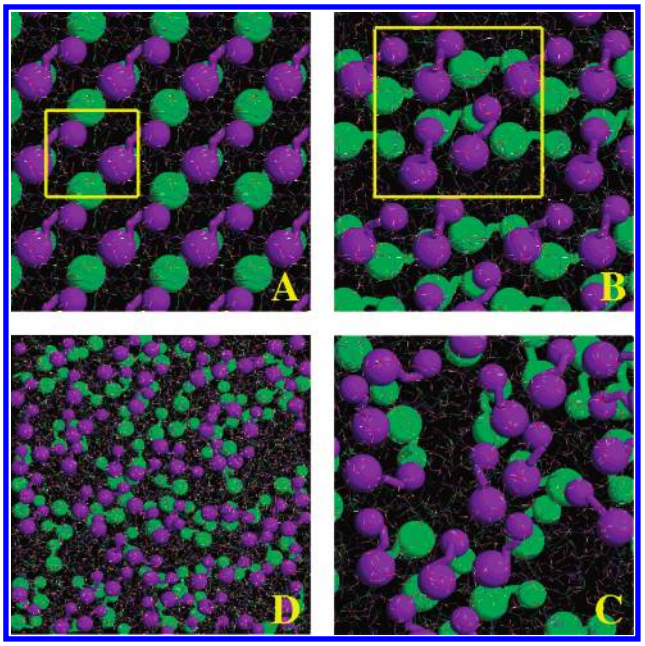

Figure 6. Snapshots from MD simulations of a hydrated DPPC bilayer with different unit-cell sizes. The simulated systems contain 1 (A), 4 (B), 16 (C), and 64 (D) lipids per leaflet. The bilayers are shown from the top, in wireframe representation, using standard coloring, except for the spacefilling representation of the headgroup phosphorus and nitrogen atoms, and the thick bonds between these atoms and the atoms connecting them. Lipids in the upper leaflet are in purple, lipids in the lower leaflet green. For the two systems with the smallest unit cells (panels A and B), the boundaries of the unit cell are indicated by yellow lines. For the two other systems (panels C and D), the whole unit cell is shown.

of about 3−5 nm deduced from the dipole−dipole correlation plots of Figure 5.

Other studies[7−11] have shown the existence of finite size effects in systems of lipid bilayers larger than the largest system studied here. However, we strongly believe that changes in structural properties observed when enlarging the system size beyond the maximal size considered in the present study arise from finite size effects of an entirely different kind; these effects are then mainly due to long-wavelength undulations of the bilayer. This is illustrated, e.g., in Figure 3 of Lindahl and Edholm (ref 8). The beginning of such undulations is indeed seen for our largest system (Figure 4F). The effect of such long-wavelength undulations could be taken into account through some mesoscopic model, by convoluting the properties calculated for an essentially flat bilayer with an appropriate function describing the distribution of orientations of such bilayer patches in a larger system. Another promising approach is hierarchical modeling, in which a small patch of a bilayer modeled at atomistic resolution is being coupled to similar patches on the basis of the mesoscopic behavior of a larger bilayer system.[40] However, such a mesoscopic approach only becomes meaningful for systems larger than the lengthscale associated with the longest-range interactions within the system (i.e., interactions between headgroup dipoles). This lengthscale is estimated in the present work to be of the order of 3−5 nm.

The second question regarding the minimum simulation length required for the reliable evaluation of the structural properties reported above will now be addressed. This point may be investigated by computing these properties over different blocks from a longer simulation. The results of such an analysis are shown in Figure 7 for the electron density profile, and in Figure 8 for the S_{CD}, with reference to the system containing

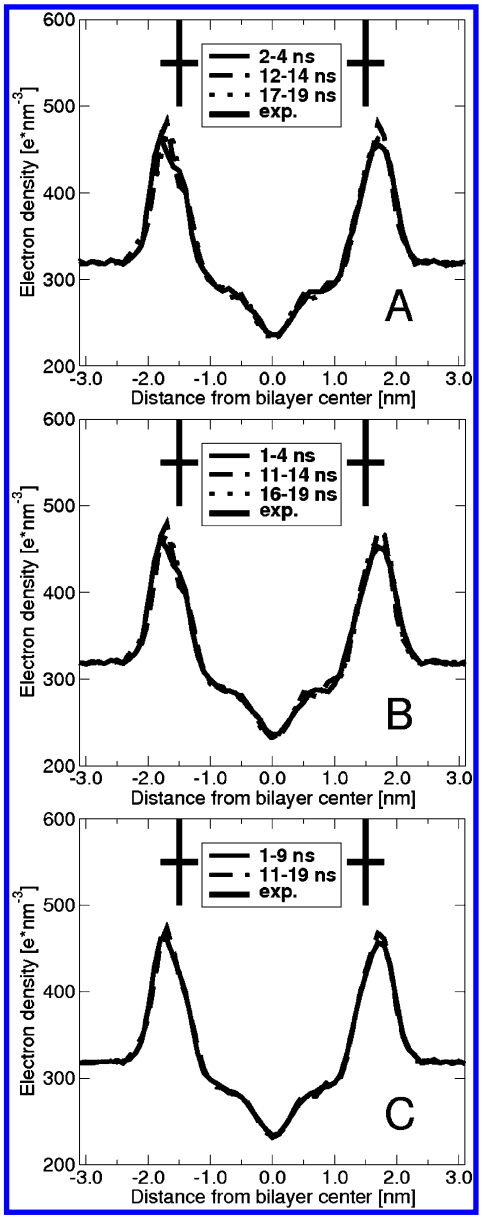

Figure 7. Electron density profiles across a hydrated DPPC bilayer averaged over different time intervals from the simulation of a system containing 36 lipids per leaflet. The lengths of the time intervals are 2 (A), 3 (B), and 8 ns (C).

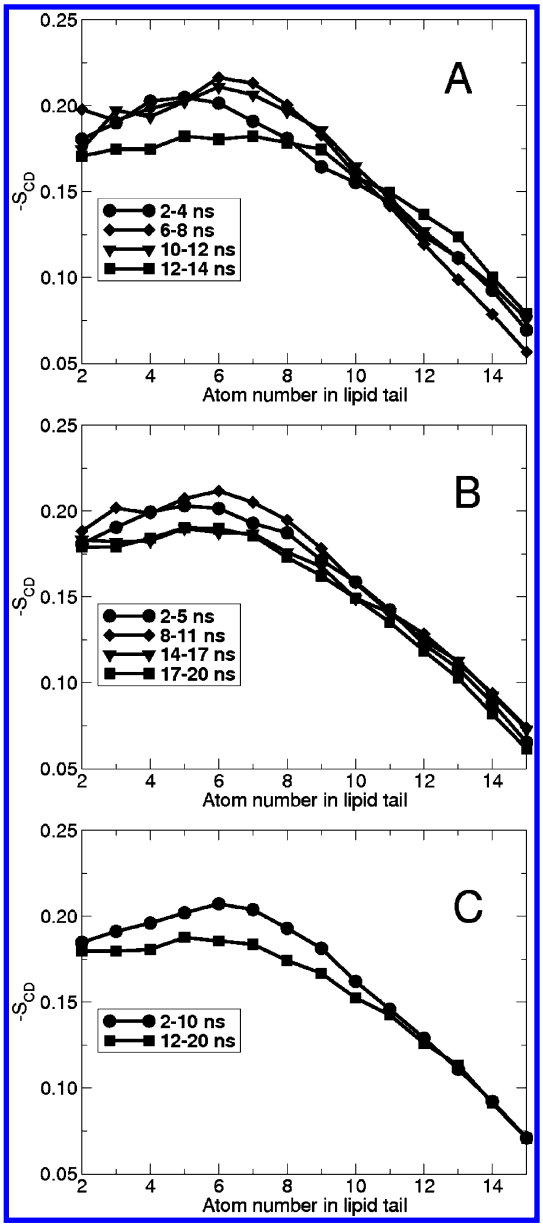

Figure 8. S_{CD} profiles for the acyl chains of a hydrated DPPC bilayer averaged over different time intervals from the simulation of a system containing 36 lipids per leaflet. The lengths of the time intervals are 2 (A), 3 (B), and 8 ns (C).

36 lipids per leaflet. These figures show the corresponding profiles obtained over different 2, 3, and 8 ns periods taken from an extended 20 ns simulation of the bilayer. In terms of the electron density profiles simulations as short as 2 ns already provide consistent results. The deviations are more important for the S_{CD} profiles, but 3 ns periods already lead to qualitatively consistent results. It may seem surprising that so short periods of time already yield converged properties in the light of recent studies showing that simulation times of at least 10−20 ns are required for the calculation of accurate bilayer properties.[11,12] In particular, these previous studies showed long correlation times and slow convergence for basic properties, such as the area per lipid in simulations under constant pressure conditions.

A possible explanation for this apparent contradiction may be that the structural relaxation of a bilayer system is intrinsically faster under constant volume conditions than under constant pressure conditions. This hypothesis was tested on the basis of two 100 ns simulations of a fully hydrated DPPC bilayer, for a system containing 64 lipids per leaflet simulated under constant volume and constant pressure conditions, respectively. The force field and system were identical in both cases (system F in ref 11) and the dimensions of the box in the constant volume simulation were chosen as the corresponding equilibrium values for the constant pressure simulation, leading to a surface tension very close to 0. The convergence properties of the surface tension in the constant volume simulation or of the bilayer area in the constant pressure simulation are compared in Figure 9, in the form of their cumulative averages and variances as a function of time. To enable direct comparison between the convergence properties of the two quantities, the time series were shifted and scaled so that both averages were 0 and both variances were 1 when calculated over the whole simulation time. Clearly, the surface tension at constant volume converges much faster to its average value than the bilayer area at constant pressure. Note also that the fluctuations in the surface tension have a much shorter period than those in the area of the bilayer. These observations support the above hypothesis that the constant volume relaxation of the surface tension is faster than

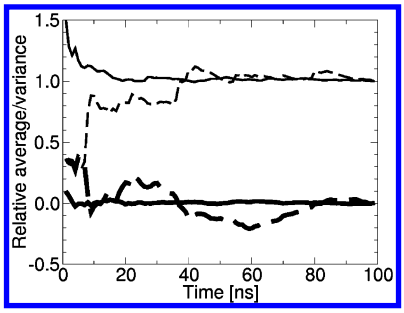

Figure 9. Cumulative average values (thick lines) and variances (thin lines) of the surface tension (solid lines) in a constant volume simulation and area of the bilayer (dashed lines) in a constant pressure simulation displayed as a function of time for a hydrated DPPC bilayer containing 64 lipids per leaflet (force field of system F in ref 11). The raw data was shifted and scaled so that both averages are zero and both variances are 1 when calculated over the whole simulation time.

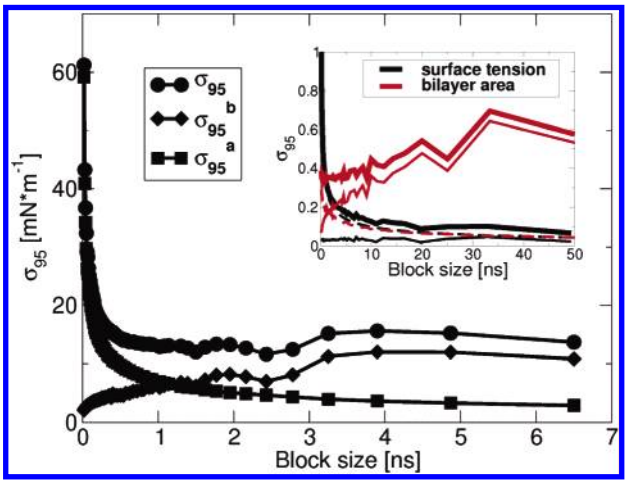

Figure 10. Error analysis concerning the time-series of the surface tension of a hydrated DPPC bilayer from a simulation of a system containing 36 lipids per leaflet. The 95% confidence interval (σ_{95}) is shown as a function of the time interval used for block averaging (circles). The components of σ_{95} (see the Appendix), namely the average 95% confidence interval (σ_{95}^{b}) associated with the error in the block averages (squares) and the 95% confidence interval (σ_{95}^{a}) associated with the error made in averaging over the block averages (diamonds), are also displayed. The inset shows the results of a similar analysis for both the surface tension at constant volume (black lines: σ_{95}, thick line; σ_{95}^{b}, thin line; σ_{95}^{a}, dashed line) and the bilayer area at constant pressure (red lines) based on two longer simulations of a bilayer containing 64 lipids per leaflet (force field F in ref 11), after the time series were shifted and scaled so that both averages were 0 and both variances were 1 when calculated over the whole simulation time.

the constant pressure relaxation of the surface area. This again suggests that constant volume simulations could be advantageous in the initial stages of force-field refinement, due to their better convergence properties.

The nature of the fluctuations in the time series of the surface tension for the constant volume simulations may be further clarified by using block averaging (see the Appendix). Figure 10 shows the 95% confidence interval (σ_{95}) in this quantity as a function of the time interval used for block averaging, as evaluated from the 20 ns simulation of the system containing 36 lipids per leaflet. The value of σ_{95} consists of two components. The first one (σ_{95}^{b}) is due to the error in the block averages themselves, while the second one (σ_{95}^{a}) is due to the error made upon averaging over the block averages. The value of σ_{95} reaches a plateau at about 0.5 ns. Such a plateau indicates that independent (uncorrelated) average values can be obtained from successive blocks of this specific length taken out of the simulation.[41] The onset of the plateau may be interpreted as a correlation time. A second plateau is reached at about 3 ns, after an increase in σ_{95}. This indicates that there is at least one second, longer correlation time present in the system. Note that a similar error analysis performed on the pressure components themselves (data not shown) essentially leads to the same results as those displayed in Figure 10 for the surface tension. Therefore, observations made there concerning the convergence behavior of the surface tension in time also pertain to the individual pressure components.

The inset in Figure 10 shows a comparison between the values of σ_{95} in the surface tension at constant volume and in the bilayer area at constant pressure for the 100 ns simulations discussed above, after the time series were shifted and scaled so that both averages were 0 and both variances were 1 when calculated over the whole simulation time. The error in the surface tension reaches a plateau value at shorter time and is smaller than the error in the bilayer area. The plateau value for the error in the surface tension is reached for blocks of about 20 ns, while the error in the bilayer area does not reach a plateau value at all on the 100 ns time scale. This observation is consistent with the development of the cumulative variance with time as shown in Figure 9. Interestingly, the errors in the surface tension and bilayer area are built up differently, as can be seen from the breakdown of σ_{95} into its components. As expected, σ_{95}^{b} decreases steadily with increasing block size for both properties, while the opposite is true for σ_{95}^{a}. For the surface tension, σ_{95}^{b} represents the leading contribution to the error up to relatively long block lengths, while σ_{95}^{a} is nearly constant. This is due to the fact that the pressure is a rapidly fluctuating property, and thus is associated with a large error when averaged over a short period of time. In contrast, for the bilayer area the error is dominated by σ_{95}^{a} for all but the shortest block lengths, because the area is a slowly fluctuating property compared to the pressure.

Although the collective structural properties monitored in the present constant volume simulations appear to converge rapidly (i.e., within a few nanoseconds), the motions of the individual lipid molecules do not necessarily converge at the same rate. The relaxation time associated with the motion of a particular lipid segment can be estimated by monitoring the corresponding autocorrelation function (ACF). The average ACFs corresponding to the orientation of the third methylene segment in the sn-1 chain of DPPC (defined by the vector perpendicular to the plane containing the second, third, and fourth carbon atoms in the sn-1 chain, counting from the ester carbon) and of the vector connecting the phosphorus and nitrogen atoms in the DPPC headgroup are shown for a number of systems in Figure 11. Error bars were determined by evaluating the ACF of the particular vector for each lipid molecule, and are drawn at the 95% confidence interval. Note that for the vectors considered here, the relaxation behavior is similar for all systems containing at least 16 lipids per leaflet. The ACF for the orientation of the third methylene segment reaches a plateau value after about 1 ns (Figure 11A). However, the rotational relaxation of the headgroups requires a much longer time. The plateau region of the ACF for the phosphorus−nitrogen vector (Figure 11B) is not even reached during the longest simulation time (20 ns for the system with 36 lipids per leaflet) considered here (data not shown). Thus, whereas collective structural properties such as the calculated electron density profile (Figure 7) essentially reach convergence within a few nanoseconds, the individual lipids have not nearly explored all possible headgroup orientations within this time span. As illustrated in Figure 12, which shows

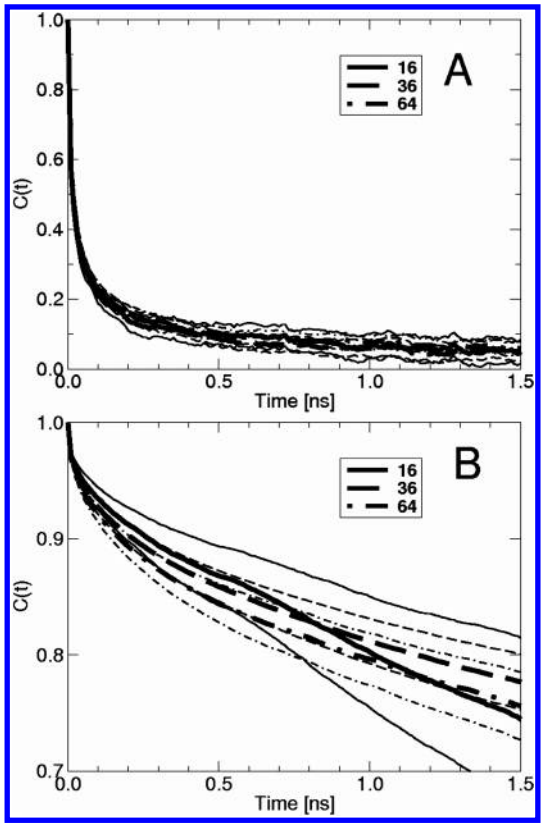

Figure 11. Time autocorrelation functions corresponding to the orientation of specific segments within individual lipids in a hydrated DPPC bilayer. The systems involve 16 (solid lines), 36 (dashed lines), or 64 (dot−dashed lines) lipids per leaflet. The thick lines represent averages over all lipids in the system. The corresponding thin lines are drawn at the 95% confidence intervals. The autocorrelation functions are calculated for the vector perpendicular to the plane defined by the second, third, and fourth carbon atoms in the sn-1 chain of DPPC (A), and for the vector connecting the phosphorus and nitrogen atoms in the headgroup of DPPC (B).

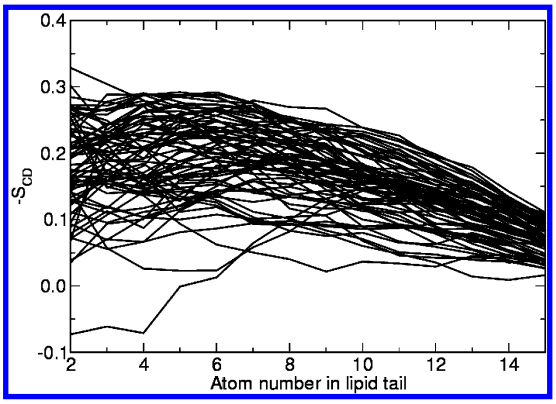

Figure 12. S_{CD} profiles for the individual sn-1 acyl chains of a hydrated DPPC bilayer, calculated for a system containing 36 lipids per leaflet, and over 3 ns of simulation.

the S_{CD} profiles of the sn-1 chain of the individual lipids in the system containing 36 lipids averaged over 3 ns, a similar observation can be made for the order parameters of individual lipids. These S_{CD} profiles show considerable spread, indicating that the individual chains sample rather different parts of the configurational space available to them.

Conclusion

The convergence of the structural and dynamical properties of a phospholipid bilayer in water as a function of the system size and simulation time was investigated by using MD simulations under periodic boundary conditions at constant volume, and applying lattice-sum electrostatics. The electron density profile, the carbon−deuterium order parameters, and the surface tension were shown to be converged for a system containing 36 lipids per leaflet simulated over a period of 3 ns (after 0.5 ns equilibration). Reasonable estimates for these properties can already be obtained from a system containing 16 lipids per leaflet. The convergence limit of 36 lipids per leaflet and the analysis of the orientational correlations between the lipid headgroups suggest a correlation length of about 3−5 nm in the lateral directions for a hydrated DPPC bilayer in the liquid-crystalline phase. Although collective properties for which experimental data are most abundant appear to be well converged in such constant volume simulations of relatively small systems performed over rather short time scales, two important restrictions should be kept in mind. First, the relaxation times associated with the motions of individual lipids can be much longer than the present simulation times, indicating that the reliable calculation of the dynamical properties of lipid bilayers certainly requires much longer simulations. Second, simulations under constant volume conditions appear to sample a much more restricted extent of phase space compared to simulations under constant pressure conditions. Therefore, the simulated observables (e.g., surface tension) converge significantly faster than the corresponding observables (e.g., bilayer area) under constant pressure conditions. This reduces the relevance of constant volume simulations for comparison with experiment, but may render them extremely useful for the initial exploration of changes in force-field parameters, changes in the types of lipids, or the inclusion of small solute molecules in a bilayer. The qualitative difference in convergence properties between constant volume and constant pressure simulations may perhaps be understood by realizing that enforcing a constant bilayer area imposes a stronger restriction in the phase space available to the system compared to enforcing a constant average pressure. This is because the area is an extensive property, which is free of fluctuations when constrained, while the pressure (or surface tension) is an intensive property, only enforced as a time-averaged constraint with fluctuations allowed. Another possible explanation is that a change in the bilayer area requires relatively large concerted motions of the lipids (and is thus slow), while large changes in the pressure can be provoked by rather small intermolecular displacements (and is thus fast). For these reasons it may be expected that it takes longer to fully explore the available phase space in constant pressure simulations than in constant volume simulations.

Appendix: Block Averaging Procedure for Evaluating Errors and Correlation Times in Simulated Properties

In MD simulations the time-evolution of a system is determined by integrating its classical equations of motions using a succession of finite time steps. A macroscopic property $\langle A \rangle$ of the system may then be estimated by averaging over the corresponding instantaneous values $A(t_i)$, $i = 1, ..., N$, associated with the N configurations sampled during the simulation. An error ϵ in the average value $\langle A \rangle$ may in principle be evaluated by using the standard statistical formula

$$\epsilon = \frac{1}{\sqrt{N}} \sqrt{\frac{\sum_{i}^{N} (A(t_i) - \langle A \rangle)^2}{N - 1}}$$

However, this standard error is usually a lower bound to the real error due to correlations among the successive data points. If the time-correlation function $C(t) = \langle A(\tau)A(\tau + t)\rangle_\tau$ can be determined, an estimate of the real error in the average can be derived. Usually, $C(t)$ is fitted to one or a sum of exponentials, with characteristic times corresponding to the correlation times in the data series.[42] In practice, however, this fitting procedure is difficult to apply (especially in the presence of very long correlation times) and the method is only approximate. An alternative method is to analyze the error in the average as a function of the time interval over which this average is taken, as suggested by Flyvbjerg and Petersen.[41] Here, we follow a slightly different approach. The time series is divided into M successive blocks of length L, with $M \cdot L \leq N$, and the average $A(K)$ of the data in the successive blocks $K = 1, ..., M$ is determined. The error in the Kth block average is

$$\epsilon_K = \frac{1}{\sqrt{L}} \sqrt{\frac{\sum_{i=(K-1)L+1}^{KL} (A(t_i) - A(K))^2}{L-1}}$$

Next, the block averages are treated as data points with a particular average uncertainty $\sigma_{95}{}^{b}(L)$. The uncertainty chosen here corresponds to the 95% confidence interval and is evaluated as

$$\sigma_{95}{}^{b}(L) = t_{95}(L) \frac{1}{M} \sum_{K=1}^{M} \epsilon_K$$

$t_{95}(L)$ is the 95th percentage point from a Student-t distribution as a function of the number of degrees of freedom L. Similarly, the 95% confidence interval $\sigma_{95}{}^{a}(M)$ in the average of the block averages is computed as

$$\sigma_{95}{}^{a}(M) = t_{95}(M) \frac{1}{\sqrt{M}} \sqrt{\frac{\sum_{K=1}^{M} (A(K) - \langle A \rangle)^2}{M-1}}$$

Finally, the 95% confidence interval in the average of the block averages, taking into account their intrinsic uncertainty, is given by

$$\sigma_{95}(M,L) = \sigma_{95}{}^{a}(M) + \sigma_{95}{}^{b}(L)$$

By analyzing the dependence of $\sigma_{95}(M,L)$ on L for a given trajectory length N (i.e., with $M = N/L$), the nature of the fluctuations in the data may be analyzed (see the inset of Figure 10 and its discussion). If σ_{95} reaches a plateau value around a given block size L, the block averages can be considered independent (uncorrelated), and a correlation time may be associated with the onset of the plateau. If multiple correlation times are present in the data, and provided that the overall trajectory length is sufficient, several plateaus may appear.

Note that the error estimate proposed above may still represent a lower bound to the real error. If correlation times longer than the overall trajectory length are present, they will not be detected. A method to assess the likelihood of longer correlation times is to monitor the cumulative average and variance of the data with time. In the absence of longer correlation times, these two quantities should show a damped oscillation around their infinite-time limits.

Acknowledgment. The authors thank Olle Edholm for a preprint of ref 10 investigating the electrostatic interactions in a DPPC bilayer for large systems. Financial support was obtained through the National Center of Competence in Research (NCCR) Structural Biology of the Swiss National Science Foundation, which is gratefully acknowledged.

References and Notes

(1) Scott, H. L. *Curr. Opin. Struct. Biol.* **2002**, *12*, 495.
(2) Armen, R. S.; Uitto, O. D.; Feller, S. E. *Biophys. J.* **1998**, *75*, 734.
(3) Petrache, H. I.; Tu, K.; Nagle, J. F. *Biophys. J.* **1999**, *76*, 2479.
(4) Pastor, R. W.; Venable, R. M.; Feller, S. E. *Acc. Chem. Res.* **2002**, *35*, 438.
(5) Sachs, J. N.; Petrache, H. I.; Woolf, T. B. *Chem. Phys. Lipids* **2003**, *126*, 211.
(6) Tristram-Nagle, S.; Nagle, J. F. *Chem. Phys. Lipids* **2004**, *127*, 3.
(7) Feller, S. E.; Pastor, R. W. *Biophys. J.* **1996**, *71*, 1350.
(8) Lindahl, E.; Edholm, O. *Biophys. J.* **2000**, *79*, 426.
(9) Marrink, S. J.; Mark, A. E. *J. Phys. Chem.* **2001**, *105*, 6122.
(10) Wohlert, J.; Edholm, O. *Biophys. J.* **2004**, *87*, 2433.
(11) Anézo, C.; de Vries, A. H.; Höltje, H.-D.; Tieleman, D. P.; Marrink, S. J. *J. Phys. Chem. B* **2003**, *107*, 9424.
(12) Patra, M.; Karttunen, M.; Hyvönen, M. T.; Falck, E.; Lindqvist, P.; Vattulainen, I. *Biophys. J.* **2003**, *84*, 3636.
(13) Egberts, E. Molecular Dynamics Simulation of Multibilayer Membranes, Thesis, University of Groningen, Groningen, The Netherlands, 1988.
(14) Egberts, E.; Marrink, S. J.; Berendsen, H. J. C. *Eur. Biophys. J.* **1994**, *22*, 423.
(15) Huang, H.; Perez, J. J.; Loew, G. H. *J. Biomol. Struct. Dynam.* **1994**, *11*, 927.
(16) Kastenholz, M. A.; Hünenberger, P. H. *J. Phys. Chem. B* **2004**, *108*, 774.
(17) Luty, B. A.; van Gunsteren, W. F. *J. Phys. Chem.* **1996**, *100*, 2581.
(18) Hünenberger, P. H.; McCammon, J. A. *J. Chem. Phys.* **1999**, *110*, 1856.
(19) Hünenberger, P. H.; McCammon, J. A. *Biophys. Chem.* **1999**, *78*, 69.
(20) Weber, W.; Hünenberger, P. H.; McCammon, J. A. *J. Phys. Chem. B* **2000**, 104, 3668.
(21) Börjesson, U. Thesis (Diss. ETH No. 15454), ETH Zürich, Switzerland, 2004; Chapter 2.
(22) Chandrasekhar, I.; Kastenholz, M.; Lins, R. D.; Schuler, L. D.; Tieleman, D. P.; van Gunsteren, W. F. *Eur. Biophys. J.* **2003**, *32*, 67.
(23) Berendsen, H. J. C.; Postma, J. P. M.; van Gunsteren, W. F.; Hermans, J. In *Intermolecular Forces*; Pullman, B., Ed.; Reidel: Dordrecht, The Netherlands, 1981; pp 331−342.
(24) van Gunsteren, W. F.; Billeter, S. F.; Eising, A. A.; Hünenberger, P. H.; Krüger, P.; Mark, A. E.; Scott, W. R. P.; Tironi, I. G. *Biomolecular Simulation*: *GROMOS96 Manual and User Guide*; BIOMOS b.v.: Zürich, Switzerland, Groningen, The Netherlands, 1996.
(25) Scott, W. R. P.; Hünenberger, P. H.; Tironi, I. G.; Mark, A. E.; Billeter, S. F.; Fennen, J.; Torda, A. E.; Huber, T.; Krüger, P.; van Gunsteren, W. F. *J. Phys. Chem. A* **1999**, *103*, 3596.
(26) Nagle, J. F.; Tristram-Nagle, S. *Biochim. Biophys. Acta* **2000**, *1469*, 159.
(27) Hockney, R. W.; Eastwood, J. W. *Computer simulation using particles*, 2nd ed.; Institute of Physics Publishing: Bristol, UK, 1988.
(28) Deserno, M.; Holm, C. *J. Chem. Phys.* **1998**, *109*, 7678.
(29) Deserno, M.; Holm, C. *J. Chem. Phys.* **1998**, *109*, 7694.
(30) Hünenberger, P. H. Lattice-sum methods for computing electrostatic interactions in molecular simulations. In *Simulation and theory of electrostatic interactions in solution*: *Computational chemistry, biophysics, and aqueous solution*; Hummer, G., Pratt, L. R., Eds.; American Institute of Physics: New York, 1999; pp 17−83.
(31) Hünenberger, P. H. *J. Chem. Phys.* **2000**, *113*, 10464.
(32) De Leeuw, S. W.; Perram, J. W.; Smith, E. R. *Proc. R. Soc. London A* **1980**, *373*, 27.
(33) Ryckaert, J.-P.; Ciccotti, G.; Berendsen, H. J. C. *J. Comput. Phys.* **1977**, *23*, 327.
(34) Berendsen, H. J. C.; Postma, J. P. M.; van Gunsteren, W. F.; DiNola, A.; Haak, J. R. *J. Chem. Phys.* **1984**, *81*, 3684.
(35) Katsaras, J. *J. Phys. Chem.* **1995**, *99*, 4141.
(36) Petrache, H. I.; Dodd, S. W.; Brown, M. F. *Biophys. J.* **2000**, *79*, 3172.
(37) Seelig, A.; Seelig, J. *Biochim. Biophys. Acta* **1975**, *406*, 1.
(38) Chandrasekhar, I.; Bakowies, D.; Glättli, A.; Hünenberger, P. H.; Pereira, C.; van Gunsteren, W. F., submitted to *Mol. Simulation*.
(39) Tironi, I. G.; Sperb, R.; Smith, P. E.; van Gunsteren, W. F. *J. Chem. Phys.* **1995**, *102*, 5451.
(40) Ayton, G. S. D.; Bardenhagen, S.; McMurty, P.; Sulsky, D.; Voth, G. A. *IBM J. Res., Dev.* **2000**, *45*, 417.
(41) Flyvbjerg, H.; Petersen, H. G. *J. Chem. Phys.* **1989**, *91*, 461.
(42) Hess, B. *J. Chem. Phys.* **2002**, *116*, 209.